

UNCLASSIFIED



DEPARTMENT OF DEFENCE

AD-A279 275

AR-008-522



2

DSTO

Land, Space and
Optoelectronics Division

RESEARCH REPORT
SRL-0144-RR

PASSIVE MILLIMETRE WAVE IMAGING:
A REVIEW

by
Philip J. Picone

DTIC

ELECTE

MAY 17 1994

S F D

94-14618



SURVEILLANCE RESEARCH LABORATORY

APPROVED FOR PUBLIC RELEASE

DTIC QUALITY INSPECTED

UNCLASSIFIED

94 5 16 077

DISCLAIMER NOTICE

THIS DOCUMENT IS BEST QUALITY PRACTICABLE. THE COPY FURNISHED TO DTIC CONTAINED A SIGNIFICANT NUMBER OF PAGES WHICH DO NOT REPRODUCE LEGIBLY.

UNCLASSIFIED

AR-008-522



SURVEILLANCE RESEARCH LABORATORY

Land, Space and Optoelectronics Division

RESEARCH REPORT
SRL-0144-RR

PASSIVE MILLIMETRE WAVE IMAGING:
A REVIEW

by

Philip J. Picone

Accession For	
NTIS CRA&I	<input checked="" type="checkbox"/>
DTIC TAB	<input type="checkbox"/>
Unannounced	<input type="checkbox"/>
Justification	
By	
Distribution /	
Availability Codes	
Dist	Avail and/or Special
A-1	

SUMMARY

The propagation of millimetre waves through the atmosphere is reviewed. Target temperature contrast and ranges possible are calculated for current passive millimetre wave detectors under various atmospheric conditions. Some possible future developments in passive millimetre wave imaging arrays are also discussed.

© COMMONWEALTH OF AUSTRALIA 1993

FEBRUARY 94

COPY No.

APPROVED FOR PUBLIC RELEASE

POSTAL ADDRESS: Director, Surveillance Research Laboratory, PO Box 1500, Salisbury, South Australia, 5108. **SRL-0144-RR**

UNCLASSIFIED

This work is Copyright. Apart from any fair dealing for the purpose of study, research, criticism or review, as permitted under the Copyright Act 1968, no part may be reproduced by any process without written permission. Copyright is the responsibility of the Director Publishing and marketing, AGPS. Inquiries should be directed to the Manager, AGPS Press, Australian Government Publishing Service, GPO Box 84, Canberra ACT 2601.

CONTENTS

	Page No
1. INTRODUCTION.....	1
2. ATMOSPHERIC MILLIMETRE-WAVE PROPAGATION.....	3
2.1 Atmospheric attenuation.....	3
(a) Rain.....	6
(b) Suspended Hydrometers (cloud, fog, haze).....	6
(c) Water vapour attenuation.....	6
(d) Dry air.....	7
(e) Turbulence.....	7
(f) Dust and sand.....	7
(g) Summary.....	8
3. RADIATION SOURCES AND DETECTION.....	9
3.1 Background mm-wave emission.....	9
3.2 Detector Noise Limits.....	10
3.3 Passive mm-wave observation.....	10
3.3.1 Background and target temperature sources.....	10
3.3.2 Temperature contrast and passive mm-wave range.....	13
4.0 MM-WAVE IMAGING DETECTORS.....	19
4.1 Current Millimetre Detectors / Systems.....	19
4.2 Detector Developments.....	20
4.2.1 Anisotropic etched Si horn arrays.....	20
4.2.2 Photonic Crystals.....	21
5. SUMMARY.....	22
REFERENCES.....	23

FIGURES

1	Major factors in mm-wave imaging system.	2
2	Specific attenuation by the atmosphere (one atm, 20°C and 7.5 g/m ³ water vapour).	4
3	One-way attenuation as a function of frequency.	4
4	Temperature components for a mm-wave radiometer.	9
5	Temperature components for a mm-wave radiometer.	11
6	Radiometric sky temperature at 35 and 94 GHz.	12
7	Temperature contrast, clear air 50% RH.	15
8	Temperature contrast, fog 0.4 gm/m ³ .	16
9	Temperature contrast, rain ~ 4mm/hr.	16
10	Temperature contrast, beam width of 1 degree, rain ~ 4 mm/hr.	17
11	Temperature contrast, clear air 50% RH.	17
12	Temperature contrast, fog 0.4 gm/m ³ .	18
13	Temperature contrast, rain ~ 4 mm/hr.	18
14	Side view of a 240 GHz horn array.	20
15	Technique to form a Photonic Crystal.	21
16	Photonic crystal forbidden gap.	22

TABLES

1	Beam width (°) at different apertures and frequencies.	1
2	Absorption ratio (α (220 GHz)/ α (35 GHz)) of phases of H ₂ O.	5
3	Attenuation at 40 GHz in Dust and Sand at various Visibilities.	7
4	Atmospheric effects at four window frequencies.	8
5	Sky temperature at different window frequencies and atmospheric conditions.	11
6	Material Emissivity at Normal Incidence.	13

1. INTRODUCTION

The possibility of passive millimetre wave (mm-wave) imaging systems based on simple array structures is discussed in this report. There have been a number of reviews concerning mm-wave or sub mm-wave research at DSTO in the past 3-4 years. Reports by Fourikis [1] and Bates [2] cover the basics of propagation of mm-waves through the atmosphere, the Australian metrological conditions and the advantages of mm-wave systems in adverse conditions. Three reports written by CSIRO [3,4,5] (under contract for DSTO) covered mm-wave propagation, setting up a mm-wave propagation experiment to measure attenuation in various weather conditions and the feasibility of using mm-waves in a portable communications link. These papers concentrated on the application and development of active radar, or communication systems using a heterodyne detector (single element) and passive imaging arrays were not reported on at length. This type of detector limits the development of simple cheap mm-wave imaging systems due to the high cost and limited availability of integrated circuits that work at these frequencies. In the past two years mm-wave integrated circuits are becoming more available but cost is still a problem. This report concentrates on passive mm-wave imaging and does not cover active mm-wave systems. For work in this area readers are referred to reports by Bates [2] and Fourikis [1].

A number of imaging systems using heterodyne detectors have been reported [13,14,15,16]. Two systems [13,15] operated in the 35 GHz (~8.5 mm) atmospheric transmission window, and two [14,16] in the 90 GHz (~3mm) window. For both frequencies single element parabolic dish antennas [13,14] and small array detectors [15,16] have been employed. Although the larger wavelength (compared to infrared imaging) results in poor spatial resolution, useful images can be obtained for the shorter mm-wave operation ($1 \text{ mm} < \lambda < 8 \text{ mm}$ or $220 \text{ GHz} > f > 35 \text{ GHz}$). When a small antenna is used the angular resolution is diffraction limited. For mm-waves the angular resolution is termed the beam width (θ_b), generally defined as the 3 dB points of the antenna radiation pattern, and for a given aperture diameter (D) and wavelength (λ) is approximated by [8,17]:

$$\theta_b = 4\lambda / \pi D \quad 1.1$$

Table 1 indicates the beam width for a number of different apertures and frequencies. From this Table, large apertures (~ 1 m) are needed for spatial resolution at low frequencies. This has implications in the design of imaging systems where small devices are required. The higher the frequency the greater the atmospheric absorption (see below) and a trade off between resolution, aperture size and detection range must be made.

Table 1. Beam width ($^\circ$) at different apertures and frequencies.

Aperture (m)	Frequency (GHz)			
	35	90	140	220
0.01	62.5	23.1	15.6	10
0.1	6.3	2.3	1.6	1
1	.63	.23	.16	.1

Appleby et al [13,20] described a parabolic dish ($D \sim 0.5$ m) radiometer with a two axis scanning system to build up an image. Considerable scan time was required to form an image with the bulk of the time needed to move and stabilise the antenna dish. This is one of the main problems when using a large dish antenna to form an image. An operating frequency of 35 GHz was used resulting in an angular resolution, as given by (1.1), of approximately 0.017 radians or 1° . With non polarised single sideband (SSB) detection a radiometer antenna noise temperature (T_n) of 1000 K was reported.

A similar system operating at 98 GHz was described by Wilson and Ibbott [14]. This was a sideways scanning radiometer mounted on a helicopter. The forward movement of the aircraft was used to construct an image along the flight path. With an antenna diameter of 0.4 m an angular resolution of $\sim 0.5^\circ$ is possible. Using orthogonal polarisation detection with two detectors, an antenna noise temperature of ~ 800 K was reported. These two examples indicate the advantages of using higher frequency for better resolution and the improved noise figure using orthogonal polarisation detection.

A commercial system operating at 94 GHz has been produced by Millitech [15]. This detector is an 8×8 array of slot line antennas. Larger arrays, up to 48×32 , have been constructed by joining the basic 8×8 unit together. For the larger array, an angular resolution of approximately 0.2° can be obtained when using a 0.63 m lens as the aperture. A nominal image frame rate of 30 Hz was also reported with pixel (or antenna) noise temperatures of 4000 K.

An array receiver operating at 35 GHz has been reported by Alder et al [16]. A monolithic silicon, 4×4 array on a 1 cm^2 chip, and a hybrid array with 25 elements have been built. These receiver arrays consist of dipole detectors or mixers, on a single high permittivity substrate. A dielectric lens, typically 100 mm diameter, is used to focus the mm wave radiation onto the detector. Typical overall noise figures (including single sideband, antenna and lens losses) of 10.5 dB were reported.

Figure 1 indicates the major factors to be considered in an mm-wave imaging system. Propagation through the atmosphere is important as absorption and attenuation governs the amount of energy reaching the detector. In the rest of this report it is intended to briefly analyse mm-wave atmospheric propagation, detection ranges possible under various atmospheric conditions and a discussion of the possible detector systems based on small arrays.

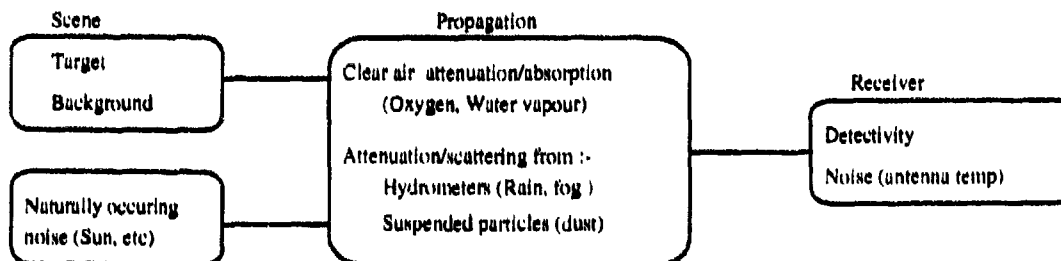


Figure 1. Major factors in mm-wave imaging system.

2. ATMOSPHERIC MILLIMETRE-WAVE PROPAGATION

The propagation of mm-waves is governed by the refractive index of the medium. For the atmosphere the refractivity (expressed in ppm) is a complex function and expressed as:

$$N = N_0 + N'(f) + jN''(f) \quad 2.1$$

where;

N_0 is the frequency independent term,

$N'(f)$ is the frequency dependent dispersion, and

$N''(f)$ is the frequency dependent absorption.

Dispersion and absorption terms arise from the molecular spectra of water and oxygen in the atmosphere.

The dispersive term, or propagation delay, produces ray bending. As the atmosphere primarily varies as a function of height, dispersion leads to elevation angle pointing errors. The largest errors occur at low elevation angles (that is near the horizon) caused by the rapid variation in the atmospheric conditions close to the earth surface. This is particularly true for transmission over water where the relative humidity, just above the surface, is high.

Millimetre wave absorption depends upon a number of factors including precipitation (rain, wet snow), suspended particles (fog, cloud, dust, haze), water vapour and turbulence. The presence of water, in different phases, is the major contributor. Extensive modelling of these factors has been reported and these will be reviewed with relevance to short range (few kilometres) passive sensing.

2.1 Atmospheric attenuation.

The basic attenuation properties of mm-waves in clear air are shown in Figure 2 [6,7]. Large absorption peaks occur at approximately 22, 60, 119, 183 and 342 GHz caused by the presence of oxygen and water vapour. Between these peaks there are transmission windows approximately centred at 35, 90, 140 and 240 GHz. These windows are used in applications that require distance transmission, for example: radar, surveillance and long range communication, while the peaks, especially 60 GHz, have been used for secure communications over a short range. The fitted curve in Figure 2 is composed of models for the absorption peaks caused by oxygen and water molecules and an empirical correction term.

The increasing interest in passive microwave sensing is in their better atmospheric transmission in adverse weather (rain/fog) conditions compared to infrared detection (Figure 3). For frequencies less than 20 GHz (or λ 's greater than 1.5cm) atmospheric effects are negligible. At the transmission window wavelengths atmospheric effects cannot be ignored. As shown in Figure 2 only transmission windows at 35, 90, 140, and 220 GHz allow sensing over large distances due to the lower absorption.

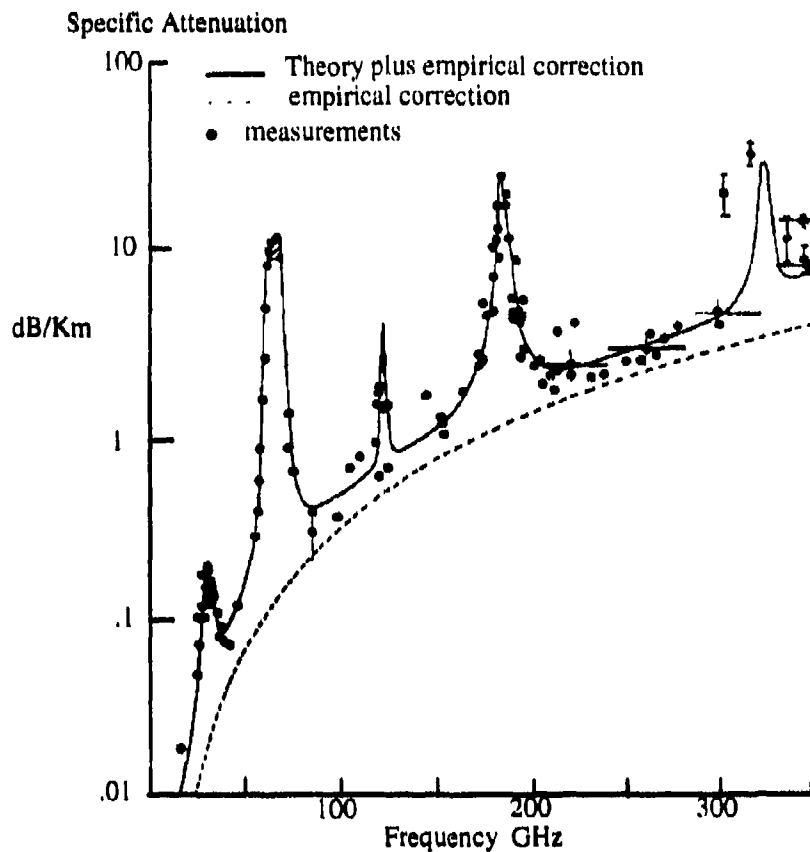


Figure 2 Specific attenuation by the atmosphere at one atmosphere, 20°C and 7.5 g/m³ water vapour density.

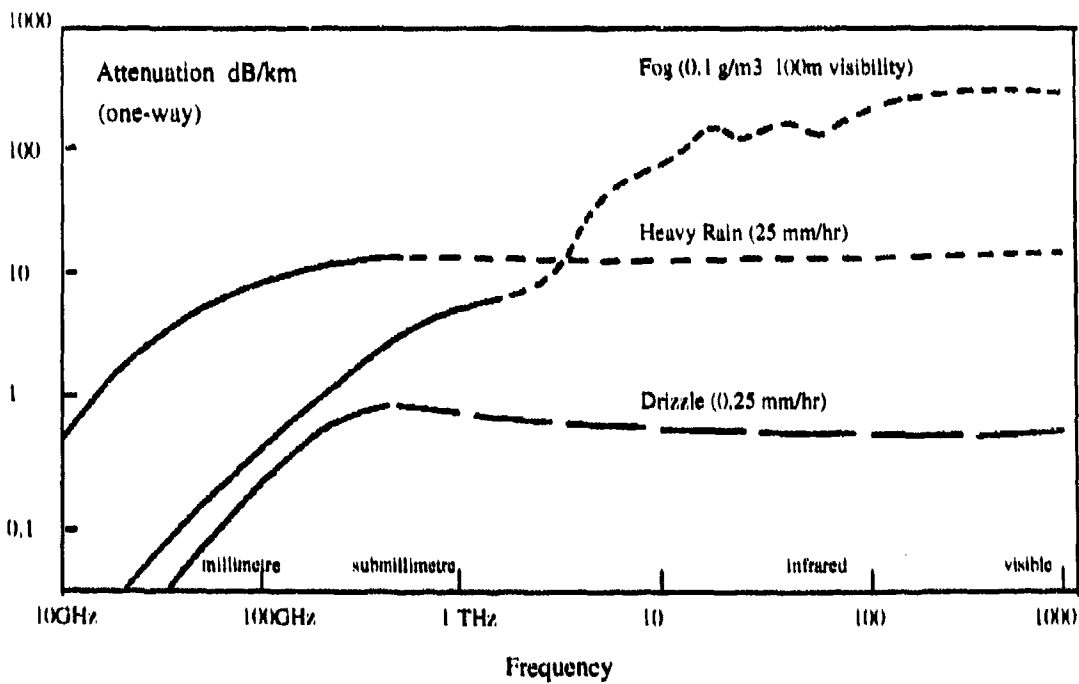


Figure 3. One-way attenuation as a function of frequency.

The total attenuation (A) in air at a given frequency is given by integrating a number of terms which describe the attenuation of different atmospheric components. This can be expressed as:

$$A = \int_0^L [\alpha_v(x) + \alpha_d(x) + \alpha_r(x) + \alpha_w(x)] dx \quad 2.2$$

where:

L is the path length,

$\alpha_v(x)$ is the specific attenuation due to water vapour,

$\alpha_d(x)$ is the specific attenuation due to dry air,

$\alpha_r(x)$ is the specific attenuation due to rain and,

$\alpha_w(x)$ is the specific attenuation due to suspended hydrometers (fog, cloud, haze).

For clear air only attenuation due to dry air and water vapour need to be considered. Both depend upon frequency, dry air pressure and temperature while $\alpha_v(x)$ additionally depends upon the water vapour concentration. Empirical models [9,10,11,12] have been developed based on the available data, and theoretical descriptions of the atmosphere, to determine the propagation of mm-waves. Empirical expressions for these attenuation coefficients have been determined and the transparency of the four atmospheric windows can be calculated for different weather conditions.

The physical state of the atmosphere can be described by five parameters; these being p, θ , v, ω and R, where;

p (= P-e) is the atmospheric pressure, P = barometric pressure, e = water vapour pressure,

θ (= 300/T) is the inverse temperature $^{\circ}\text{K}^{-1}$,

v (= $7.219e\theta$ or $\text{RH} = 29e\theta^{18}$) is the water vapour concentration (gm/m^3) or relative humidity (RH),

ω is the liquid water concentration gm/m^3 , and

R is the rain rate (gm/m^3).

Water in its different phases, vapour \rightarrow liquid, is the dominant contribution to the attenuation in the transparent windows. The specific attenuation of H_2O phases increases with frequency as shown in Table 2 [12].

Table 2 Absorption ratio (α (220 GHz)/ α (35 GHz)) of phases of H_2O .

Absorption ratio	Rain	Suspended hydrometers	Moist air
α (220 GHz)/ α (35 GHz)	5	16	24

Hydrometers (cloud, fog, rain, hail) can be represented by small dielectric scatterers with size ranges from a few microns (cloud) to a few centimetres (hail). Simple spherical shapes are easily modelled, however the real life complex shapes are difficult. Ice and snow are extremely difficult and crude

approximations are generally used. A number of models have been developed to describe the size distribution of hydrometers to calculate mm-wave scattering and absorption. The use of these simpler models is adequate for the estimation of attenuation with the use of parameters to agree with the measured data.

The different phases of water are all modelled differently; these being,

(a) Rain.

Rain presents the most serious limitation to mm-wave transmission through the atmosphere and is generally modelled by:

$$\alpha_r = aR^x \text{ dB/km} \quad 2.3$$

where the coefficients a and x are frequency dependent parameters and calculated from the different models of rain droplet size and size distribution. Rainfall average and rain cell extent for a local area needs to be acquired over a number of years. This is required by the model to determine the expected attenuation in that area. Snow is very difficult to model due to the variation in shapes and orientations possible, but this is generally not required in Australian conditions.

(b) Suspended Hydrometers (cloud, fog, haze).

This is generally modelled by Rayleigh scattering of small dielectric particles and approximated by:

$$\alpha_w = b\theta^y \text{ dB/km} \quad 2.4$$

where b and y are frequency dependent parameters. Suspended hydrometers generally have less attenuation than rainfall, but have a strong temperature (θ) dependence. Cloud attenuation in the 140 and 220 GHz bands can rival rainfall attenuation dependent upon the cloud path that is encountered. The effect of rain and fog on the oneway attenuation across the frequency spectrum is shown in Figure 3. This graph shows the advantage of mm-wave transmission, compared to IR, particularly in fog conditions.

(c) Water vapour attenuation.

For frequencies below 400 GHz there exist 3 discrete strong water vapour attenuation lines at 22, 183 and 342 GHz. Within the windows the attenuation is given by:

$$\alpha_v = c(p/101)v\theta^y = c'(p/101)RH\theta^{-17} \text{ dB/km} \quad 2.5$$

where c , c' and y are frequency dependant parameters. There is also a large contribution to the water vapour absorption at frequencies less than 400 GHz caused by very strong absorption lines at THz frequencies. These lines have absorption tails that extend down to these lower frequencies. This is usually modelled by a continuum for these frequencies and given by:

$$\alpha_z = k(p/101)v^x\theta^y(f/100)^z \text{ dB/km} \quad 2.6$$

where k , x , y and z depend upon the fitting profile of the H_2O absorption lines.

(d) Dry air

There is also a small contribution, except at absorption lines, from dry air which is mainly a contribution from oxygen molecules. This is given by:

$$\alpha_d = dp\theta^3 \text{ dB/km} \quad 2.7$$

where d is a frequency dependent term.

(e) Turbulence.

Small scale fluctuations in the refractivity can cause scintillation in the propagation of RF waves. The scintillation affects the amplitude, phase and angle of arrival of the signal. For passive imaging this will result in a blurring of the scene. It is more pronounced at low elevation angles where the signal path traverses the more turbulent region of the atmosphere leading to problems for observations in the horizontal plane. Strong turbulence and refractivity changes due to humidity variations close to the sea surface are to be expected. Over land, turbulence would be expected at hot atmospheric temperatures as indicated by the 'shimmering' observed at visible wavelengths. Turbulence may not be a major problem when observations are primarily in the vertical plane over short ranges.

(f) Dust and sand.

There has been little work on the propagation of millimetre or microwave radiation through dust or sand storms, with most work concentrating on microwaves with frequencies less than 10 GHz. Dust or airborne sand particles are modelled as small dielectric scatterers with permittivity ϵ and an effective radius a_e which is related to the particle size distribution. The attenuation (α_{sd}) is given by:

$$\alpha_{sd} = 188.7(a_e / \lambda) \cdot (G / V_o) \text{ dB/km} \quad 2.8$$

where G is related to the complex permittivity, V_o is the optical visibility (km) and λ the wavelength [33]. Calculations and measurements of attenuation at 40 GHz through dust and sand storms show a large discrepancy, with the theory greatly underestimating the attenuation (Table 3).

Table 3. Attenuation at 40 GHz in Dust and Sand at various Visibilities [33].

Approximate Visibility km	Measured attenuation @ 40 GHz dB/km	Calculated attenuation for various moisture contents.		
		5% RH	10% RH	20% RH
0.7	0.164	0.041	0.066	0.078
2.0	0.115	0.027	0.0435	0.051
3.0	0.0875	0.021	0.033	0.039
4.0	0.0684	0.015	0.024	0.0294

Even using high water vapour contents (the measurements were in Saudi Arabia where RH can get to 20%), there is a large disagreement with the measured attenuation. It was suggested that a variation in the dust particle size distribution over the test path (14 km) was the source of the disagreement. Further, in the event of dust storms large variations in the meteorological conditions occur which lead to excessive

scintillation in the received signal. This may also contribute to the excess measured attenuation. The attenuation would be expected to increase for higher frequencies (shorter wavelengths) as shown in equation 2.8. The typical attenuation for a 40 GHz signal is of the order of 0.1 dB/km which is similar to the attenuation experienced in thick fog (Table 4). As the dust/sand is primarily a surface layer it should not effect the 'sky' temperature to any great degree.

(-) Summary.

The attenuation of mm-waves in the atmosphere by various phases of H₂O can be calculated with an empirical model and a number of parameters (p , θ , v , ω and R) which describes the local atmospheric conditions. These equations and frequency dependent parameters have been consolidated into a computer model in which representative or average atmospheric conditions can be modelled. A zenith path can be modelled by assuming a height profile for the atmospheric parameters, and this is represented by:

$$A_z = \alpha_r L_r + b_z \omega + c_z v + d_z \quad 2.9$$

where ω and v are integrated over the height profile ie;

$$\omega = \int_0^{\infty} \omega(h) dh \quad \text{and} \quad v = \int_0^{\infty} v(h) dh \quad 2.10$$

For short paths as used in passive surveillance, a set of average conditions for the local area can be assumed and the specific attenuation coefficients (α) simply multiplied by the path length (L) to find the total attenuation. In this way variations in the atmosphere (both horizontally and vertically) are simply averaged. A summary of the one-way attenuation at four frequencies for different atmospheric effects [18] is shown in Table 4. The effects of turbulence cannot be taken into account.

Table 4. Atmospheric effects at four window frequencies.

Parameter	One-way loss (dB/km)			
	35 GHz	94 GHz	140 GHz	220 GHz
Clear air 50% RH	0.11	0.46	1.0	3.0
Clear air 100% RH	0.22	1.08	2.43	6.39
Rain (mm/hr)				
0.25	0.06	0.34	0.50	0.59
1.0	0.23	0.99	1.29	1.50
4.0	0.92	2.84	3.35	3.73
16.0	3.67	8.16	8.66	9.30
Cloud.				
rain	5.14	35.04		
dry	0.50	3.78		
Fog (g/m ³)				
0.01 (light)	0.006	0.04	0.07	0.12
0.10 (thick)	0.06	0.38	0.68	1.16
1.0 (dense)	0.63	3.84	6.76	11.58
Snow (0°C)	0.007	0.0028		

3. RADIATION SOURCES AND DETECTION.

3.1 Background mm-wave emission.

In passive mm-wave imaging systems the source of the radiation must be considered. Blackbody radiation is described by Planck's law.

$$W(\lambda, T) = 2\pi hc^2 / \lambda^5 (e^{hc/\lambda kT} - 1) \quad 3.1$$

At low temperatures thermal sources are poor emitters, although the peak emission does occur at long wavelengths. For example at 1 K the peak in the blackbody curve is at approximately 100 GHz. As the temperature rises the peak in the blackbody curve moves increasingly to shorter wavelengths (300 K ~ 10 μ m Figure 4).

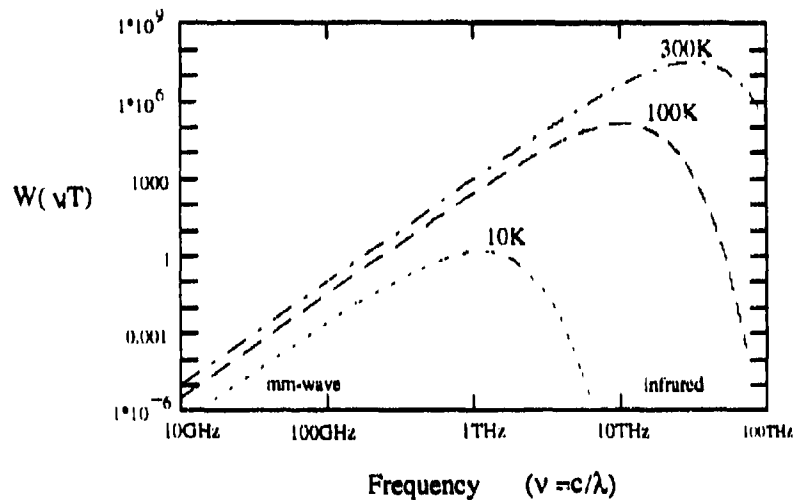


Figure 4. Blackbody spectrum at 300, 100 and 10 K

In the long wavelength "tail" of the distribution ($h\nu < kT$), the emission increases approximately linearly with temperature. This results in a large difference in spectral radiance between IR and mm-wavelengths. Since the emission of millimetre radiation by bodies at ambient temperature is low and increases only slightly with increasing temperature, it is difficult to detect objects at mm-wavelengths based on their temperature differences unless the range is very short. Instead the emissivity of materials is used to provide the contrast between objects and the background. Metal objects have an emissivity (ϵ) of zero, and consequently reflect incident mm-waves while background materials (vegetation, rock, sand etc) have an $\epsilon \sim 0.8$ (Table 6) and mainly absorb incident mm-wave radiation. If the sky is the primary source of the mm-wave radiation, that is, the sky temperature is reflected into the detector by the object, considerable temperature contrast between metallic objects and backgrounds is possible. With a water background the contrast is less as the emissivity of water is approximately 0.5 (Table 6). The contrast arises because the reflected sky temperature is very low compared to the ambient background (depending on atmospheric conditions as expanded later). Thus in general, the reflection of the sky temperature off an object is used for detection with metallic objects appearing 'cold' in a 'warm' background. Conversely, when looking into the sky, an aeroplane will appear 'warm' in a 'cold' background as the object reflects

the ground temperature. The atmospheric conditions limit the temperature contrast and also attenuate the transmission of mm-waves, which governs the detection range. As a reflection off the target is required for detection, a physically large target can appear quite small if no surface is efficiently reflecting the 'sky' (or ground for airborne targets) towards the detector. Because of this, horizontal surveillance is not very effective and mm-wave systems have generally been mounted on airborne platforms so that the 'sky' is reflected back towards the detector system.

3.2 Detector Noise Limits.

The operating temperature of a radiometer is given by;

$$T_{op} = 2(T_a + T_r) \quad 3.2$$

where T_a is the antenna temperature and $T_r = (F-1)T_o$, the effective temperature of the receiver. F is the system noise figure and T_o , a standard noise temperature (typically 290°K). For a total power radiometer the S/N (Signal to Noise) can be written as [18];

$$S/N = 2(\Delta T_a / T_{op})^2 (B_{if} / 2B_N) \quad 3.3$$

where B_{if} and B_N are the intermediate frequency and post detection bandwidth's respectively. The thermal sensitivity (minimum detectable rms temperature ΔT_m) of a total power microwave radiometer is given by setting $S/N = 1$ [13,18]. Thus ΔT_m is;

$$\Delta T_m = T_{op} / \sqrt{B_{if} / 2B_N} \quad 3.3$$

For an ideal background limited receiver ($T_r = 0$) $T_{op} = 2T_a$ and has a maximum sensitivity of approximately 0.2 K for a 500 K blackbody calibration source with a post detection bandwidth (B_N) of 100 Hz (10 msec integration time) and a radio frequency bandwidth (B_{if}) of 4 GHz. Generally, typical receivers have noise temperatures of around 2000 K and maximum sensitivities between 0.1 and 1 K depending upon the radio frequency bandwidth and the post detection bandwidth.

3.3 Passive mm-wave observation.

3.3.1 Background and target temperature sources.

The power received by a mm-wave radiometer is generally expressed as an effective temperature. This can be related to the effective power by using equation 3.4.

$$P = k_B T B_{if} \quad 3.4$$

When observing a target with a radiometer the received signal temperature is composed of a number of components including emission from the objects in the antenna beam, atmospheric emission and reflected sky emission, such that:

$$T_{rec} = T_t + T_{hg} + T_{sun} \text{ (K)} \quad 3.5$$

where T_{rec} is the received temperature, T_t is the target temperature, T_{bg} is the background temperature and T_{atm} is the atmospheric temperature. This is shown diagrammatically in Figure 5 where the target temperature is composed of T_{rs} , the reflected sky temperature, and T_{obj} the object temperature.

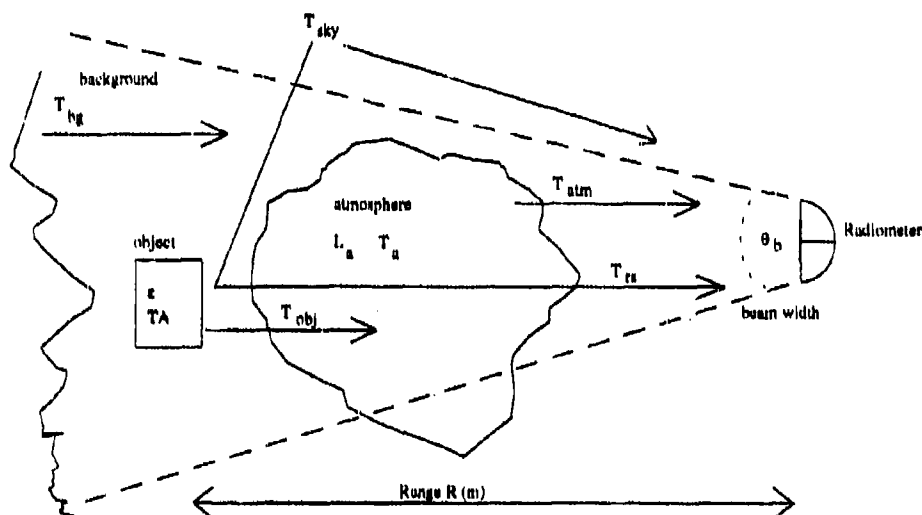


Figure 5. Temperature components for a mm-wave radiometer.

The energy absorbed by the atmosphere is re-radiated as blackbody radiation and is often known as sky noise. This has an equivalent sky brightness temperature T_{sky} such that:

$$T_{sky} = T_{atm} \left(1 - \frac{1}{L_z}\right) + \frac{T_{cb}}{L_z} \quad 3.6$$

where T_{cb} = cosmic background temperature (2.8°K) and L_z is the total zenith attenuation. The sky temperature varies as a function of atmospheric conditions and frequency as shown in Table 5. This Table shows that at the higher frequencies (> 95 GHz) and in adverse weather conditions the sky temperature becomes quite high. This limits the temperature contrast of a target and reduces the range of passive detection. A 'rule-of-thumb' [18] for mm-wave sensors with antenna diameters less than 15 cm is that passive operation is practical only up to 40 GHz due to this sky warming effect.

Table 5. Sky temperature at different window frequencies and atmospheric conditions.

Sky conditions	T_{sky} K			
	35 GHz	95 GHz	140 GHz	220 GHz
Clear	20	50	120	150
Over-cast	50	150	150	180
Fog	80	180	190	200
Light Rain	110	210	220	230
< 4mm/hr				
Moderate rain	130	240	260	270
>4 mm/hr				

As the atmospheric path varies with angle of elevation, the effective sky temperature also varies as shown in Figure 6 for 35 and 90 GHz. This effect also limits the contrast between the target and the background, particularly when angles close to the horizon are used. Since the sky is warmer at higher frequencies, contrast is less at these wavelengths and frequencies above 90 GHz become less practical for imaging in poor weather conditions.

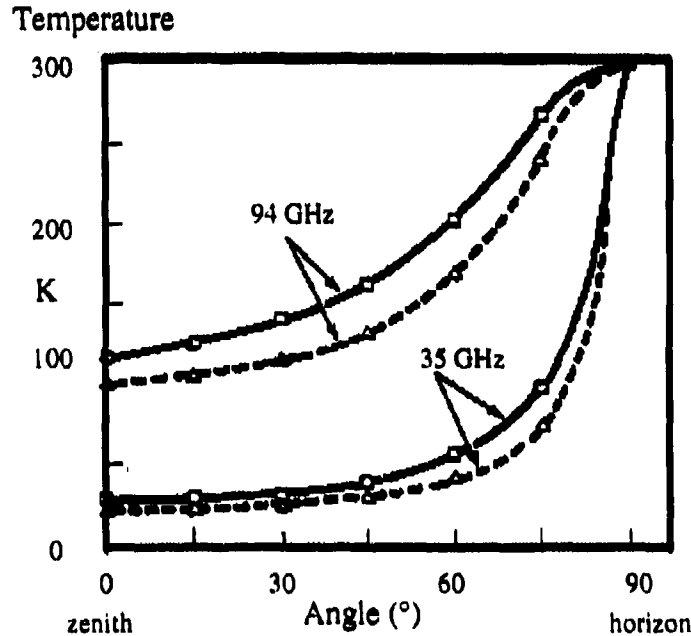


Figure 6 Radiometric sky temperature at 35 and 94 GHz, theoretical. Δ , 50% relative humidity(RH); \square 75% RH.

The temperature component of a target is given by:

$$T_{obj} = \epsilon T \quad 3.7$$

where: ϵ is the emissivity and T is the physical target temperature. The object also reflects the sky temperature and is modified by the reflectivity $(1-\epsilon)$ of the object such that:

$$T_{rs} = (1-\epsilon)T_{sky} \quad 3.8$$

The two terms, T_{obj} and T_{rs} , are the effective temperature of a target in the background. The received target signal is modified by the atmospheric absorption (L_a) between the target and receiver and can be written as:

$$T_i = (\epsilon(T - T_{sky}) + T_{sky}) / L_a \quad 3.9$$

where the atmospheric absorption is given by:

$$L_a = 10^{(\alpha R / 10)} \quad \alpha = \text{attenuation (dB/km)} \quad 3.10$$

$R = \text{range (m)}$

Similarly the background signal is composed of the background temperature and the reflection of the sky temperature such that:

$$T_{bg} = (\epsilon_b T_b + (1 - \epsilon_b) T_{sky}) / L_a \quad 3.11$$

3.3.2 Temperature contrast and passive mm-wave range

The emissivity of targets and background varies depending upon the object as shown in Table 6. Metal targets have an emissivity of ~0, and thus metal target temperatures are primarily a reflection of the sky temperature, while for background vegetation (sand, gravel concrete etc) $\epsilon \sim \geq 0.8$ and the temperature is primarily the emission of the background.

Table 6. Material Emissivity at Normal Incidence [19].

Material	emissivity	Material	emissivity
Sand	0.90	Smooth rock	0.75
Asphalt	0.83	Dry grass	0.91
Concrete	0.76	Dry snow (28-75 cm thick)	0.88-0.76
Plowed ground	0.92	Metal	0.00
coarse gravel	0.84	Fresh water (35 GHz)	0.45
Heavy vegetation	0.93	Fresh water (94 GHz)	0.59

By subtracting equations 3.9 and 3.11 the temperature difference (temperature contrast ΔT_c) between a target and a natural background (vegetation etc, temperature T) is given by:

$$\begin{aligned} \Delta T_c &= (T_t - T_{bg}) \text{ assume } T = T_{bg} \\ \Delta T_c &= [T_{bg}(\epsilon - \epsilon_{bg}) + T_{sky}(\epsilon_{bg} - \epsilon)] / L_a \end{aligned} \quad 3.12$$

The maximum contrast is obtained for a metal target ($\epsilon = 0$) in a background where $\epsilon_{bg} = 1.0$. In this situation ΔT_{max} is given by:

$$\Delta T_{max} = (T_{sky} - T_{bg}) / L_a \quad 3.13$$

As the sky temperature increases and approaches the background temperature in poor weather conditions, the maximum available contrast, and hence range decreases. From Table 5, sky temperatures of around 200 K or above are found in conditions of fog and light rain for all frequencies greater than 95 GHz. This makes passive mm-wave detection at these frequencies strongly weather dependent.

The above expressions are valid if the target completely fills the antenna beam width and the antenna has 100% efficiency. In practice this does not occur and the temperature contrast is modified by the ratio of target area to antenna area (fill factor, ϕ) and the antenna efficiency (η). The fill factor is given by:

$$\phi = 4A / (\pi R^2 \cdot \tan^2(\theta_b)) \text{ for } 0 \leq \phi \leq 1. \quad 3.14$$

where A is the target cross-section area (m^2) and θ_b the beam width (Defined as -3dB points of the main beam). Substituting these two terms into equation 3.12 results in an expression for the temperature contrast of a target.

$$\Delta T_c = \phi \eta [T_{bg}(\epsilon - \epsilon_{bg}) + T_a(\epsilon_{bg} - \epsilon)] / L_a \quad 3.15$$

Using this expression (3.15) graphs of temperature contrast (ΔT_c) as a function of range (R) for different atmospheric conditions and antenna diameters can be calculated. Figures 7 to 13 show the temperature contrast between a metal target ($\epsilon = 0$, effective scattering area = $5 m^2$ and at ambient temperature) for a number of different atmospheric conditions. In each case a background temperature (ambient) of 300 K has been assumed. A small target area ($5 m^2$) is used to approximate the limited area of the target that reflects the sky to the detector. An average emissivity (Table 6) of $\epsilon_{bg} = 0.85$ is assumed for a natural background. In all cases the antenna efficiency is set at 90%, and in Figures 7,8 and 9 an antenna aperture of 0.15m is used to model a portable detector system. In Figure 10 the beam width θ_b at each frequency is set to 1 degree, resulting in antenna diameters of 0.625 m at 35 GHz down to 0.099 m at 220 GHz.

This data shows that the beam fill factor (ϕ) is a primary factor in determining the range of passive mm-wave detection with a small antenna. The narrower the beam width (θ_b see Table 1), hence the greater the beam fill factor, the larger is the detected temperature contrast. In an optical system this is equivalent to the target filling the instantaneous field of view, that is, the target is fully resolved. For a constant antenna diameter this results in the higher frequencies having greater range, almost irrespective of the atmospheric attenuation and the increase in sky temperature with frequency. If a set beam width is specified, an operating frequency of 35 GHz offers a larger range, although a larger antenna has to be used to get the equivalent spatial resolution. The antenna size may be reduced if superresolution techniques are used. These techniques have been applied to a 35 GHz mm-wave imaging system [35] with an improvement in the spatial resolution by a factor of two with a minimal increase in the signal to noise. With larger antennas there are still problems in forming images (scanning) and in portability.

Theoretical imaging ranges in different conditions can be estimated using Figures 7 to 13 and assuming a typical temperature sensitivity of a receiver (ΔT_m) of 0.5K. For a 0.15 m aperture antenna (Figure 7,8,9), ranges out to 1700 m can be obtained for 95, 140 and 220 GHz operating frequencies in 'ideal' (minimum sky temperature and attenuation) conditions (Figure 7). At 35 GHz ranges of approximately 600 m are possible. In poor conditions (fog and rain, Figures 8 and 9) the range is reduced to around 1200 - 1300 m for an operating frequency of 220 GHz and much less for the lower frequencies. At 35 GHz a range of around 500 m is possible. For a small antenna aperture the atmospheric attenuation has little effect on the possible range. When a much larger antenna is used for 35 GHz (0.625m), a range out to 2000 m is obtained which is compared to approximately 500 m in similar conditions (rain ~ 4 mm/hr) for a 0.15 m diameter antenna.

For larger antenna diameters (> 1 m) that may be fixed to aircraft (for example a helicopter), operating frequencies of 35 or 90 GHz offer advantages in adverse weather conditions due to the lower atmospheric attenuation at the lower frequencies. This is shown in Figures 11, 12 and 13 which have the same conditions as Figures 7, 8 and 9 except that the antenna diameter is now 1.25 meter. Note that in Figures 11, 12 and 13 the range axis is between 2000 - 6000 meters compared to 500 - 3000 in Figures 7, 8 and 9. In clear air conditions (Figure 11) with low atmospheric attenuation, the higher frequencies still have the greatest range with all frequencies having ranges greater than 5000 m. Once the atmospheric attenuation increases, in fog (Figure 12) and rain (Figure 13), the affect on the temperature contrast becomes apparent with the lower frequencies having the better range. Ranges between 3500 - 5000 m and 3000 - 4000 m are found for all frequencies in fog and rain respectively.

Thus in summary ranges less than 1700 m are obtained in all conditions when small antenna diameters are used. For a small antenna diameter the beam fill factor (ϕ) has the greatest affect on range, thus for a man portable system it is best to operate in the high frequency windows. The higher atmospheric attenuation and increased sky temperature at the higher frequencies only slightly affects the range. However for large antennas (> 1 m) the atmospheric attenuation has the greatest affect on the range and the lower operating frequencies begin to have the greater range.

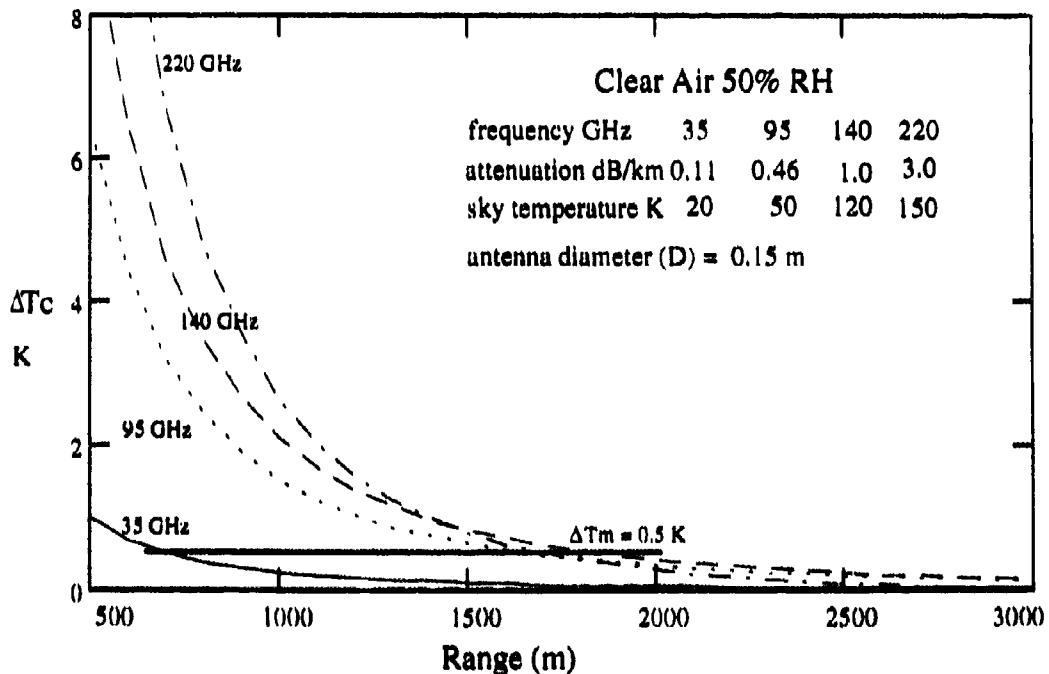


Figure 7. Temperature contrast, clear air 50% RH.

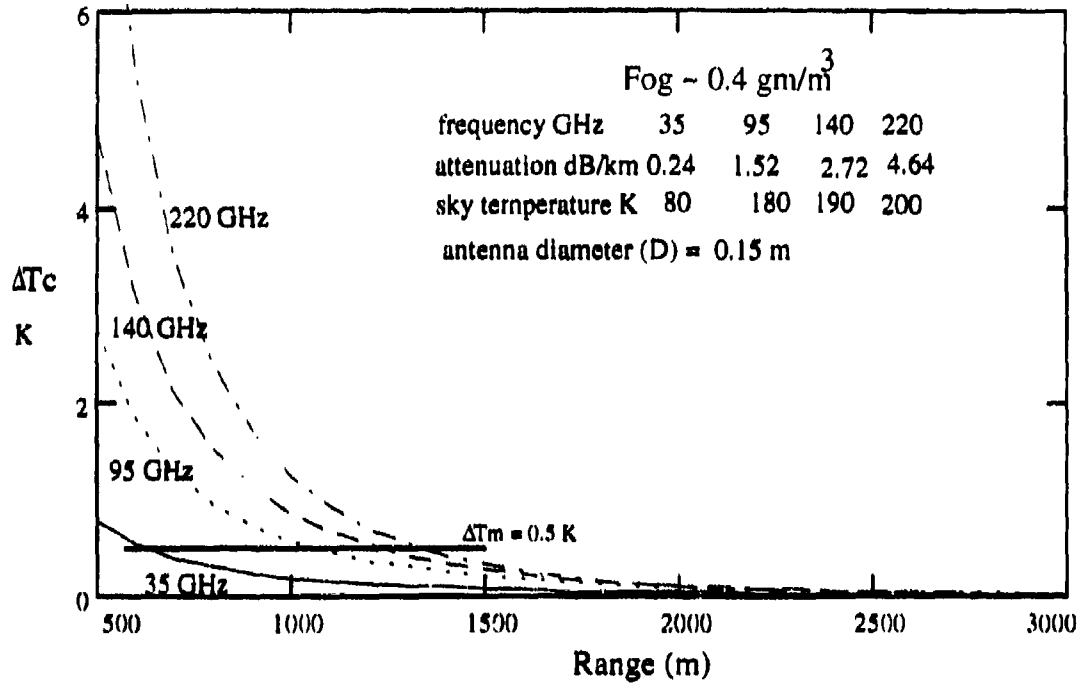


Figure 8. Temperature contrast, fog 0.4 gm/m³.

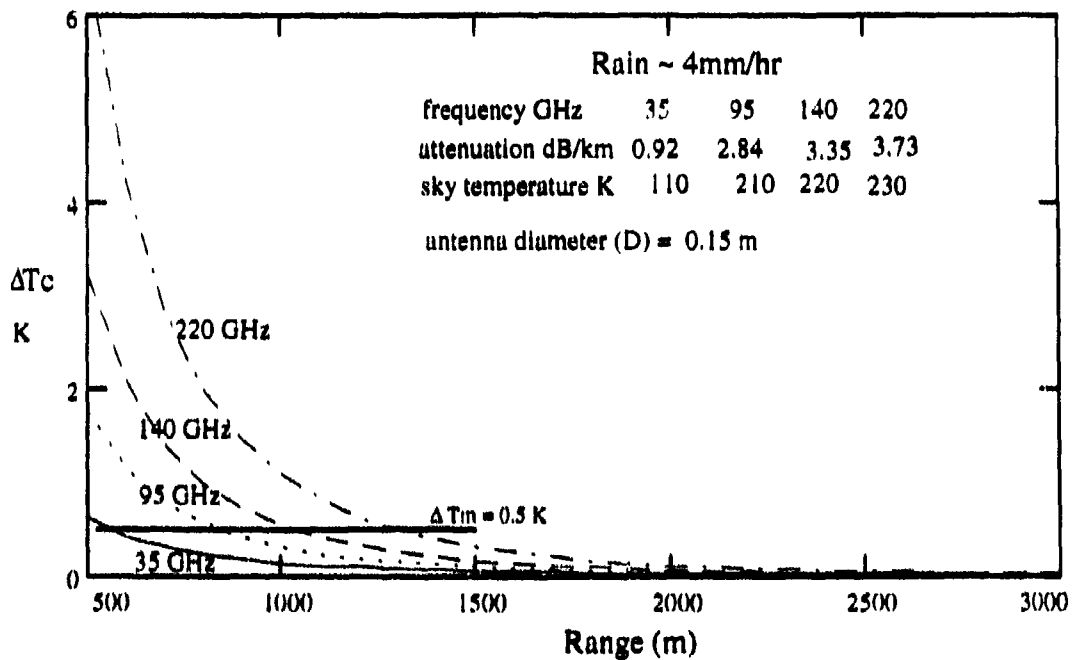


Figure 9. Temperature contrast, rain ~ 4mm/hr.

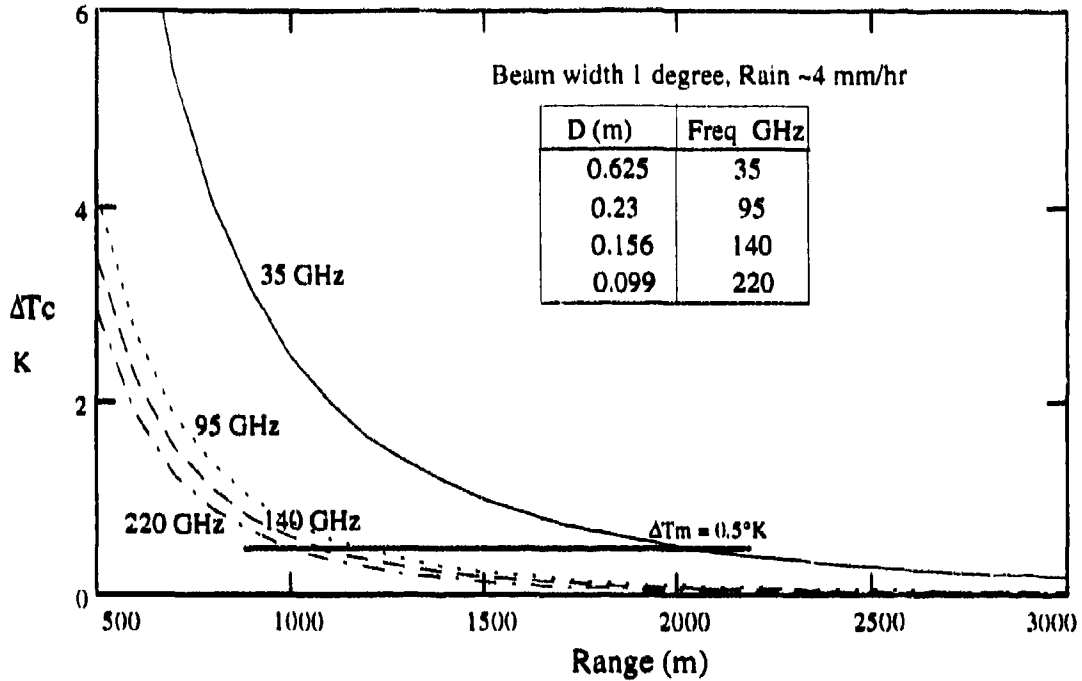


Figure 10. Temperature contrast, beam width of 1 degree, rain ~ 4 mm/hr.
(attenuation and sky temperature as figure 9)

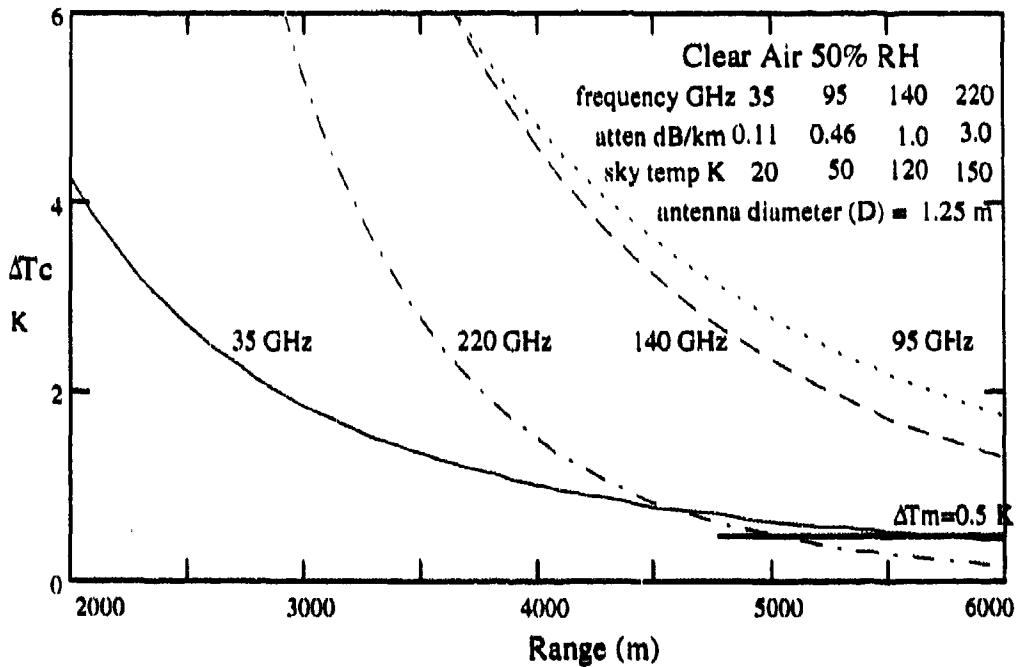


Figure 11. Temperature contrast, clear air 50% RH.

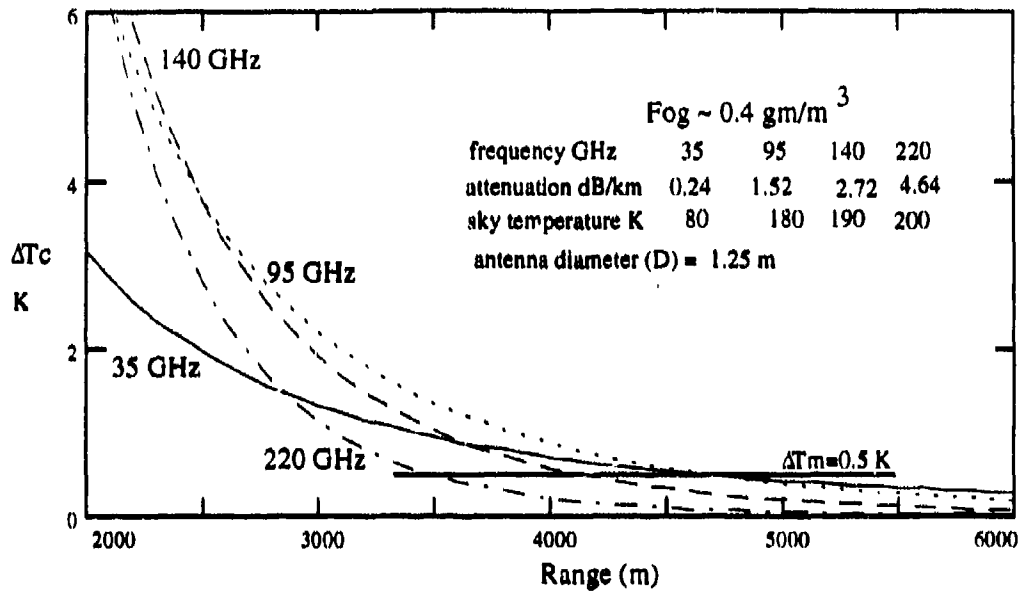


Figure 12. Temperature contrast, fog 0.4 gm/m³.

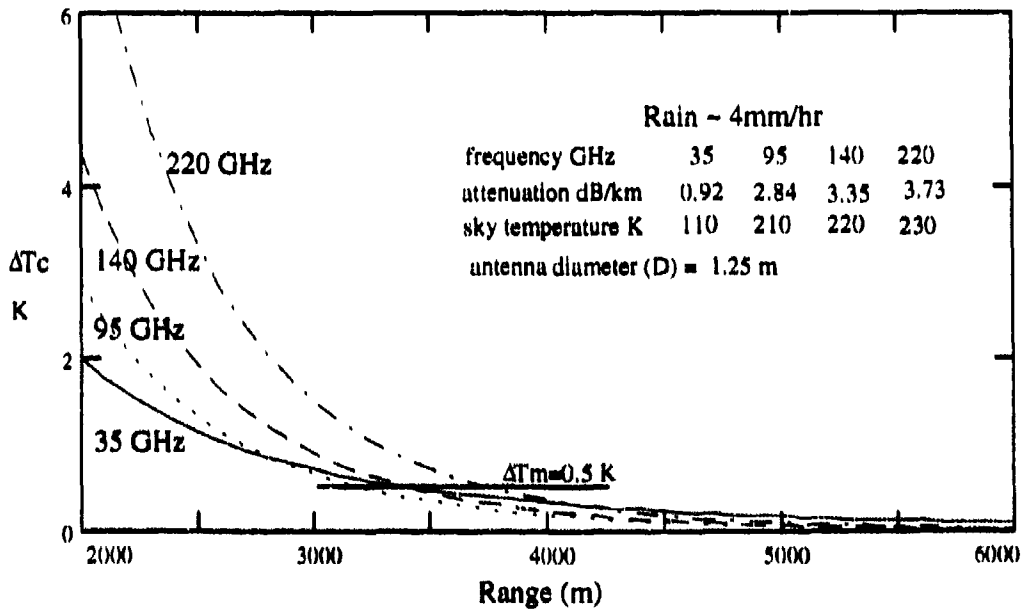


Figure 13 Temperature contrast, rain ~ 4 mm/hr

4.0 MM-WAVE IMAGING DETECTORS

4.1 Current Millimetre Detectors / Systems.

Present millimetre wave imaging systems that have been reported have used heterodyne detectors [13,14,15,16]. Two systems [13,15] operated at 35 GHz ($\lambda \sim 8.5$ mm), and two [14,16] at 90 GHz ($\lambda \sim 3$ mm). For both frequencies single element parabolic dish antennas [13,14] and small array detectors [15,16] have been employed.

Two single element detectors with parabolic antennas have been reported. Appleby et al [13,20] described a parabolic dish ($D \sim 0.5$ m) radiometer with a two axis scanning system to build up an image. An operating frequency of 35 GHz resulted in an angular resolution of approximately 17.5 mrad or 1° . Non-polarised single sideband detection resulted in an antenna noise temperature (T_n) of 1000 K and a temperature sensitivity of 0.3 K. A similar system, a sideways scanning radiometer mounted on a helicopter, operating at 98 GHz was described by Wilson and Ibbott [14]. The forward movement of the aircraft was used to construct the image along the flight path. With an antenna diameter of 0.4 m an angular resolution of $\sim 0.5^\circ$ is possible. Using orthogonal polarisation detection with two detectors, an antenna noise temperature of between 1000 and 1250 K and an rms temperature sensitivity < 0.8 K was reported. These two examples indicate the advantages of using higher frequency for better resolution.

Two array systems have also been described, one has a number of small antennas stacked together while the second has a small array of detectors and a lens to focus the mm-wave radiation. The first, a commercial system operating at 94 GHz has been produced by Millitech [15]. The basic unit is an 8x8 array of slot line antennas with a large aperture lens (0.63 m). Larger arrays, up to 48x32, have been constructed by joining the basic unit together. For the larger array, an angular resolution of approximately 0.2° can be obtained. A nominal image frame rate of 30 Hz was also reported with pixel noise temperatures of 4000°K . In the second system two types of arrays have been built. A monolithic silicon, 4x4 array on a 1cm^2 chip, and a hybrid array with 25 elements operating at 35 GHz has been reported by Alder et al [16]. These receiver arrays consist of dipole detectors or mixers, on a single high permittivity substrate. A dielectric lens, typically 100 mm diameter, is used to focus the mm wave radiation onto the detector. An overall noise figure, SSB, IF, antenna and lens losses, of 10.5 dB ($T_n \sim 3000$ K) were reported.

The main disadvantage of the single detector, parabolic dish, imaging system is the time required to scan the scene to form an image. The array systems have overcome this problem to some degree but with a higher noise figure and consequently will have a shorter range. All of the systems have used heterodyne detection with the resultant problems of high cost of electronics and high power requirements. For example the 8x8 basic unit of the commercial system requires 22 watts of electrical power.

4.2 Detector Developments.

There has been a number of developments which may lead to improvements in mm-wave detector arrays. These would require further research and development to ascertain their applicability to passive mm-wave imaging.

4.2.1 Anisotropic etched Si horn arrays.

These are small horn arrays that are etched into silicon and have been around for some years [21,22,23,24,25]. The basic horn structure is shown in Figure 14, which is a 2 layer stack for 240 GHz operation. The size of the arrays depend upon the operating frequency (wavelength) and a system operating at 90 GHz would require 4 layers. The opening is approximately 1.5λ (5 mm at 90 GHz, 1.5 mm at 240 GHz), consequently systems operating at 35 GHz ($1.5\lambda = 12$ mm) would require over 8 layers and would be virtually impossible to build. As such these arrays are only feasible for frequencies greater than 90 GHz.

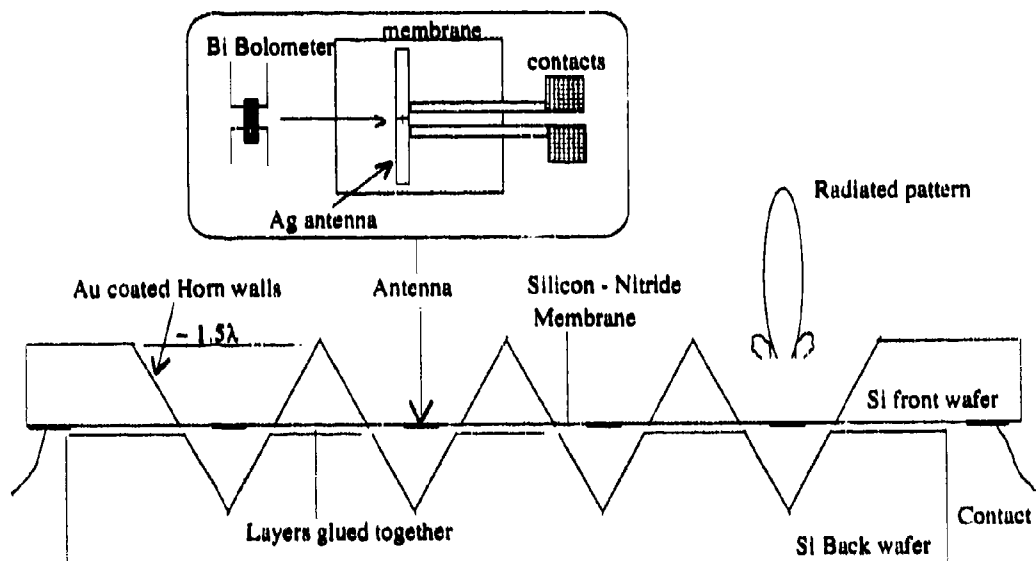


Figure 14. Side view of a 240 GHz horn array.

The pyramidal cavities, formed by anisotropic etching, forms the horn antenna with efficiencies of around 70% obtained with gold coated side walls. A detector is patterned part way through the horn as the receiving element. The detector is generally a half wave dipole antenna with a thin film bismuth bolometer [27] as the resistive detector element. (Insert in Figure 14). BiSb thermocouples [28] have also been used as the detector. These may be preferred as they are 'self biasing' and have lower noise. Schottky diodes [32] could also be used which would improve the sensitivity, then the electronics required for heterodyne detection is needed. This technology is similar to the DSTO developed metal film bolometer infrared detector [34], and could be readily established in Australia with the addition of a quarter wave dipole antenna. The advantages of the bolometer or thermocouple detector is the simplistic nature of the detector although the sensitivity may not be sufficient for passive detectors [26].

4.2.2 Photonic Crystals.

These materials are a recent development [29,30,31] and consist of an artificial three-dimensional periodic structure. The reason for the construction of 'photonic crystals' is to mimic the behaviour and properties of electron waves in real crystals by electromagnetic waves (ie optical, millimetre, microwaves etc) in a 'crystal' structure. The property of interest was the prospect of a photonic band gap, a frequency band in three dimensional dielectric structures in which electromagnetic waves are forbidden irrespective of the propagation direction. Photonic crystals [29] are made by making a series of holes to form a periodic lattice (Figure 15) in a dielectric material, for example GaAs or an epoxy.

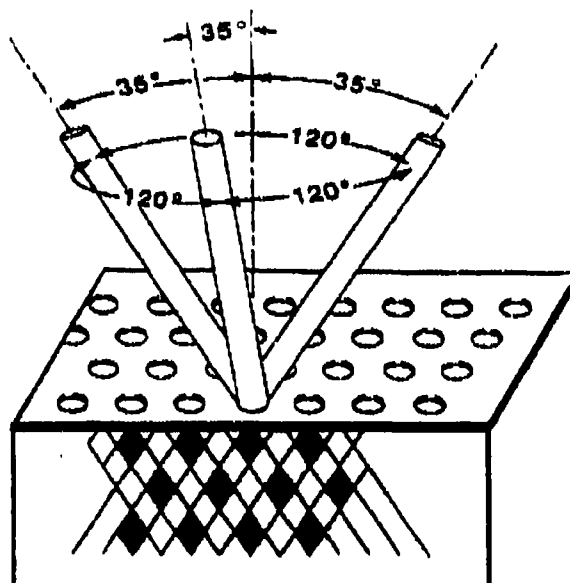


Figure 15. Technique to form a Photonic Crystal.

The hole spacing, and size, depends on the centre frequency of the band gap but they must be of the same order as the wavelength of the radiation. Thus for mm-waves a photonic crystal is made by simply drilling millimetre size holes. Figure 16 shows the microwave attenuation as a function of frequency for a photonic crystal with voids 7.8 mm apart [29]. A forbidden gap is clearly seen and falls between 13 and 16 GHz (23 - 19 mm). A second feature is also evident in this diagram. Defects in the crystal structure can lead to acceptor and donor states similar to semiconductors.

One application has been to use a photonic crystal as a substrate for a microwave antenna [31]. Previously using semiconductor substrates, for example semi-insulating GaAs, approximately 98% of the microwave energy is absorbed into the substrate and not radiated into the air. Using a photonic crystal, with a band gap shown in Figure 16 as a substrate, a bow tie antenna radiated almost all of a 13.2 GHz signal fed into the antenna as radiation at this frequency is forbidden to propagate into the crystal. Thus these crystals may be fabricated into very efficient mm-wave antennas. Further, construction of photonic crystals in semiconductors may allow the integration of electronics and antenna on the same chip for use with microwave or mm-wave detectors and imaging systems.

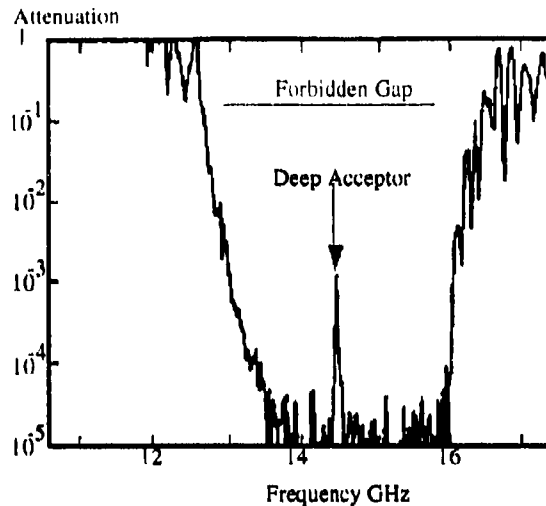


Figure 16. Photonic crystal forbidden gap.

5. SUMMARY

The use of passive mm-wave imaging systems is greatly dependent upon the operational conditions that the system needs to operate in. The greatest advantage of mm-wave over IR occurs in fog, cloud and rain. Considering the area where surveillance is required in the ADF's area of interest, that is Northern Australia, there is very little incidence of fog conditions. Some fog conditions have been modelled as they have similar atmospheric attenuation compared to dust or sand storms, where the attenuation coefficients are not well understood, and similar ranges (in an initial approximation) can be expected. Rain is experienced more often and in Fourikis's report [1] rain fall rates of 1, 5, and 10 mm/hr are exceeded 2%, 0.5% and 0.2% of the total time respectively. These rates are mainly exceeded in the wet season (approximately November to March) and only occur over small areas, ie storm cells. Thus there are limited times when passive mm-wave imaging systems will be of benefit compared to the higher resolution IR systems.

The other advantage of passive mm-wave detection is its ability to detect ambient temperature metal targets in natural backgrounds by the reflection of the 'cold' sky temperature. This could be used in conjunction with IR systems as a means to reduce the false alarm rate, or as a cuing system. The modelling has indicated that large antennas (>1m) and low operating frequencies (35 or 95 GHz) will give the greater range (~ > 4000m), however it will have the smallest spatial resolution. For man portable systems (antenna diameter < 0.2m) the higher operating frequency (240 GHz) has the larger range (~ 1500m) and the highest spatial resolution. The poor resolution may not be an overwhelming problem if large structures, for example buildings, are to be detected.

REFERENCES

- 1 N.S. Fourikis. Proposals for mm-wave systems of interest to ADF and for investigations related to the definition of their military roles in the Australian environment. Task Report DST87/144.1. Sept 1990.
- 2 B.D. Bates. Millimetre-wave characteristics, applications and technology: a review. ERL - 0495 - TM, Nov 89
- 3 L.H. Loew Mm-wave propagation (A report to DSTO contract # AE8903-F1)
- 4 K.J. Greene On the setting up of a millimetre-wave propagation experiment. (Discussion paper for DSTO contract # AE8903-P3)
- 5 J.S. Kot and L.H. Loew Feasibility study into the use of millimetre-wave antenna technology in a portable communications link. DSTO contract # AE8903-P1)
- 6 R.K. Crane. Fundamental limitations caused by RF propagation. Proc. of the IEEE, Vol 69 #2 1981 pp 196-209.
- 7 R.A. Bohlander., R.W. McMillian. and J.J. Gallagher. Atmospheric effects on near - millimetre - wave propagation. Proc. of the IEEE, Vol 73 #1 1985 pp 49 - 60.
- 8 G. Schaerer. A comparison of thermal imaging at microwave and infrared wavelengths. Infrared Physics Vol 15 1975. pp 125 - 131.
- 9 H.J. Liebe. Atmospheric EHF window transparencies near 35, 90, 140, and 220 GHz. IEEE trans. on antennas and propagation. Vol AP-31 #1 1983 pp 127 - 135.
- 10 H.J. Liebe. Tropospheric absorption and dispersion of millimetre and submillimetre waves. IEEE trans. on antennas and propagation. Vol AP-31 #1 1983 pp 221 - 223.
- 11 H.J. Liebe. The atmospheric water vapour continuum below 300GHz. Int J of infrared and millimetre waves. Vol 5 #2 1984. pp 207 - 227.
- 12 H.J. Liebe. An updated model for millimetre wave propagation in moist air. Radio Science. Vol 20 #5 pp1069 - 1089.
- 13 R. Appleby. and A.H. Lettington. Passive millimetre wave imaging. Electronics & Communication Engineering Journal. Feb 1991 PP 13 - 16.
- 14 W.J. Wilson. and A.C. Ibbot. Millimetre-wave imaging sensor data evaluation. JPL Publication 87-16 May 1987.
- 15 Millitech In Microwaves and RF. July 1992 pp113 - 116. (MM waves aid commercial applications)
- 16 C.J. Adler, C.R. Brewitt-Taylor, R.J. Davis, M. Dixon, R.D. Hodges, L.D. Irving, H.D. Rees, J. Warner. and A.R. Wedd. Microwave and millimetre-wave staring array technology. IEEE MTT-S Int Microwave Symposium, Boston June 1991. pp 1249 - 1252.
- 17 E.K Reedy and G.W. Ewell Infrared and mm-waves V4 Millimetre Systems. Editors Button and Wiltse. Academic Press 1981.

- 18 C.R. Seashore Infrared and mm-waves V4 Millimetre Systems. Editors Button and Wiltse. Academic Press 1981.
- 19 J. Kjellgren, G. Stenstrom and A Sume IR and mm-waves V15. Millimetre components and Techniques. Part VI. Editor: K.J. Button.
- 20 R. Appleby, D.G. Gleed, R.N. Anderton and A.H. Lettington High-performance passive millimetre-wave imaging. Optical Engineering June 1993 V32 pp 1370 - -1373.
- 21 Youg Guo, K. Lee, P. Stimson, K. Potter and D. Rutledge. Aperture efficiency of integrated - circuit horn antennas. Microwave and Optical Technology Letters. Jan 1991 Symposium.
- 22 G.M. Rebeiz, D.P. Kasilingham, Yong Guo, P.A. Stimson and D.B. Rutledge. Monolithic millimetre-wave two - dimensional horn imaging arrays. IEEE transactions on antennas and propagation. V 38 #9 1990 pp 1473 - 1482.
- 23 G.V. Eleftheriades, W.Y. Ali-Ahmad, L.P.B. Katehi and G.M. Rebeiz. Millimetre-wave integrated-horn antennas: Part I - Theory. IEEE transactions on antennas and propagation. V 39 #11 1991 pp1575 - 1581
- 24 W.Y. Ali-Ahmad, G.V. Eleftheriades, L.P.B. Katehi and G.M. Rebeiz. Millimetre-wave integrated-horn antennas: Part II - Experiment. IEEE transactions on antennas and propagation. V 39 #11 1991 pp1582 - 1586
- 25 N.A. Foss, P.W. Kruse Jr. , and R.A. Wood. Monolithic Integrated Dual Mode, IR/Mm-wave Focal Plane Sensor. United States Patent. # 4 654 622. March 31 1987.
- 26 P.A. Stimson. Private communication
- 27 D.P. Neikirk, W.W. Lam and D.B. Rutledge Far-infrared microbolometer detectors. Int Journal of Infrared and millimetre waves. V 5 1984 pp 245 - 278
- 28 D.P. Neikirk and D.B. Rutledge Self-heated thermocouples for far-infrared detection. Applied Physics Letters V41(5) 1982 pp 400 - 402
- 29 E. Yablouovitch. Photonic band-gap structures. J of the Optical Society of America. V10 #2 1993 pp 283 - 295
- 30 E. Yublouovitch, and T.J. Gmitter, R.D. Meade, A.M. Ruppe, K.D. Brommer and J.D. Joannopoulos Donor and Acceptor modes in Photonic band structures. Physical Review Letters. V67 # 24 1991 pp 3380 - 3383
- 31 E. Yublouovitch, and T.J. Gmitter. Photonic band structure: The face-centred-cubic case. Physical Review Letters. V63 # 18 1989 pp 1950 - 1953
- 32 W.Y. Ali-Ahmad, W.L. Bishop, T.W. Crowe and G.M. Rebeiz A 250 GHz planar low noise schottky receiver. Int Journal of Infrared and millimetre waves. V 14 (4) 1993 pp 737 - 748
- 33 Adel A. Ali and M.A. Alhuider Millimetre wave propagation in Arid land - A field study in Riyadh. (+ references cited). IEEE Trans. on Antennas and Propagation V40 1992 pp492 - 499.
- 34 K.C. Liddiard Infrared Physics. Vol 24 #1 Jan 1984 pp 57 - 64
- 35 D.G. Gleed and A.H. Lettington Application to superresolution techniques to passive mm-wave images. SPIE 1567. Applic. of digital image processing XIV p 65-72

DISTRIBUTION LIST

Defence Science and Technology Organisation

Chief Defence Scientist	}	1 shared copy with CDS
Central Office Executive		
Counsellor, Defence Science London		Control Sheet
Counsellor, Defence Science Washington		Control Sheet
Senior Defence Science Advisor		1 copy
ASSA		1 copy
Scientific Advisor, Navy		1 copy
Scientific Advisor, Air Force		1 copy
Scientific Advisor, Army		1 copy
Scientific Advisor, Polcom		1 copy

Surveillance Research Laboratory, DSTO

Director	1 copy
Chief, Land, Space and Optoelectronics Division	1 copy
Research Leader, Optoelectronics Sensors & Systems	1 copy
Head, Smart Sensors (K Liddiard)	1 copy
P.J. Picone	2 copies

Libraries and Information Services

OIC, Technical Reports Central Library Campbell Park	1 copy
Manager, Document Exchange Centre, Defence Information Services	1 copy
Defence Research Information Centre, United Kingdom	2 copies
National Technical Information service, United States	2 copies
Director Scientific Information Services, Canada	1 copy
Ministry of Defence, New Zealand	1 copy
National Library of Australia	1 copy
Defence Science and Technology Organisation Salisbury, Research Library	2 copies
MRL Maribyrong Library	1 copy
ARL Fisherman's Bend, Library	1 copy
Library DSD	1 copy
AGPS	1 copy
British Library, Document Supply Centre	1 copy

Spares

Defence Science and Technology Organisation Salisbury, Research Library	6 copies
---	----------

THIS IS A BLANK PAGE

Department of Defence
DOCUMENT CONTROL DATA SHEET

Page Classification
UNCLASSIFIED

Privacy Marking/Caveat
(of Document)
N/A

1a. AR Number AR - 008 - 522	1b. Establishment Number SRL - 0144 - RR	2. Document Date February 94	3. Task Number DST 94/454
---------------------------------	---	---------------------------------	------------------------------

4. Title PASSIVE MILLIMETRE WAVE IMAGING: A REVIEW	5. Security Classification	6. No of Pages	24
	U/C Document S (Secret)	U/C Title C (Conf)	U/C Abstract R (Rest) U (Unclass)
* For UNCLASSIFIED docs with a secondary distribution LIMITATION, use (L) in document box.			
8. Author(s) Phillip J. Picone.	9. Downgrading/Delimiting instructions N/A		
10a. Corporate Author and Address Surveillance Research Laboratory PO Box 1500 Salisbury SA 5108	11. Officer/Position responsible for Security.....N/A..... Downgrading.....N/A..... Approval for Release.....DSRL.....		
10b. Task Sponsor			

12. Secondary Distribution of this Document

APPROVED FOR PUBLIC RELEASE

Any enquiries outside stated limitations should be referred through DSTTC, Defence Information Services, Department of Defence, Anzac Park West, Canberra, ACT 2600

13a. Deliberate Announcement

No Limitation

13b. Casual Announcement (for citation in other documents)

No Limitations

14. DEFTTEST Descriptors

Millimetre waves, Detectors, Atmospheric propagation

15. DISCAT Subject Codes

2014

16. Abstract

The propagation of millimetre waves through the atmosphere is reviewed. Target temperature contrast and ranges possible are calculated for current passive millimetre wave detectors under various atmospheric conditions. Some possible future developments in passive millimetre wave imaging arrays are also discussed.